Robust URLLC Link Adaptation via Statistical Modeling of Time-Varying SINR Deviations

Shubham Kumar Baranwal[†], Ugrasen Singh[*], Member, IEEE, and Manav Bhatnagar[†], Senior Member, IEEE
[†]Department of Electrical Engineering, IIT Delhi, India
[*]Department of Electronics Engineering, IIT-ISM Dhanbad, Jharkhand, India
E-mails: {eey237520, manav}@ee.iitd.ac.in, ugrasen@iitism.ac.in

***Abstract*—This paper proposes a robust link adaptation (LA) framework for ultra-reliable low-latency communication (URLLC) under time-varying interference and noise conditions. A statistical model is developed to characterize the distribution of signal-to-interference-plus-noise ratio (SINR) deviations across consecutive time slots in a non-stationary environment. Leveraging this model, a dynamic backoff selection mechanism is designed to mitigate the impact of adverse SINR fluctuations and ensure stringent URLLC reliability requirements. In contrast to conventional approaches that rely solely on instantaneous SINR estimates, the proposed method incorporates the probability of unfavorable SINR deviations into transmission rate selection. Furthermore, analytical results reveal that the effective beamforming gain at the URLLC receiver degrades with an increasing number of interferer transmit antennas and decreasing noise variance. Extensive Monte Carlo simulations corroborate the accuracy of the proposed model and demonstrate the effectiveness of the developed LA scheme.**

***Index Terms*—Backoff, link adaptation, SINR variability, ultra-reliable low-latency communication, time-varying interference.**

I. Introduction

Ultra-reliable and low-latency communication (URLLC) is a key enabler of 5G and beyond networks, supporting applications such as industrial automation, intelligent transportation, remote surgery, and autonomous aerial vehicles. Its stringent reliability and latency requirements necessitate robust physical-layer design, effective interference management, and adaptive link optimization [1]. Link adaptation improves wireless reliability by selecting the modulation and coding scheme (MCS) based on channel state information (CSI) [2], [3]. However, channel variations may render the reported CSI outdated at transmission time, causing the selected MCS to violate the target reliability. To mitigate this issue, adaptive MCS is commonly combined with automatic repeat request (ARQ) and hybrid ARQ (HARQ). Existing works have enhanced MCS/HARQ performance through CSI and feedback error-aware MCS selection [2]–[5]. Nevertheless, these approaches primarily target throughput maximization rather than stringent reliability guarantees. Moreover, HARQ retransmissions introduce additional latency, which can result in information outage in delay-sensitive URLLC applications [6].

Existing studies have also considered signal-to-interference-plus-noise ratio (SINR) variability, but often overlook the effects of time-varying interference. The impact of such interference in factory environments is investigated in [7], providing a foundation for SINR-aware link adaptation in non-stationary settings; however, the analysis relies on ergodic capacity metrics and neglects short-packet communication. In [8], an interference distribution prediction framework is proposed for URLLC in non-stationary environments, assuming slowly varying interference. Similarly, [9] employs extreme value theory to predict interference power distributions but does not account for mobility-induced SINR variations. The work in [10] utilizes SINR variability arising from mobility and time-varying interference for backoff selection; however, a general analytical framework for reliability evaluation under diverse network conditions remains unavailable. These limitations motivate the development of a statistical framework that characterizes SINR fluctuations and enables analytical reliability evaluation in the presence of time-varying interference.

Backoff selection for link adaptation under time-varying interference has been investigated in [12], [13]. In [12], the distribution of the SINR is utilized to optimize the backoff in an interference-limited scenario, whereas [13] focuses on a noise-limited regime and adapts the transmission rate to satisfy a target reliability constraint. However, both works are restricted to specific operating conditions and do not provide a unified framework that accounts for environments with both stochastic interference and noise. The main contributions of this work are summarized as follows: i) We analyze the joint impact of time-varying interference and additive white Gaussian noise (AWGN) on the reliability of URLLC links in non-stationary environments. ii) The statistical distribution of SINR variations across consecutive time slots is derived analytically. iii) Based on the proposed analysis, the effects of interference variability, noise power, and the number of transmit antennas on the required backoff and achievable transmission rate are analytically quantified.

The remainder of this paper is organized as follows. Section II describes the system model for the URLLC link under time-varying interference and noise. Section III presents the proposed link adaptation framework, including backoff design and statistical characterization of SINR variations. Section IV provides numerical results and discusses the impact of interference and noise on system reliability. Finally, Section V concludes the paper and outlines future research directions.

II. System Model

A multi-antenna eNodeB (eNB-1) serves a user equipment (UE) under URLLC requirements in a non-stationary environment. The non-stationarity arises due to time-varying interference from a neighboring eNodeB (eNB-2). Both eNBs are equipped with N_t transmit antennas and operate with a frequency reuse factor of 1, thereby sharing the same radio resources. The eNB-2 serves multiple UEs in a time-division duplexing (TDD) mode, scheduling only one UE per time slot. For analytical tractability, a single dominant interferer is considered, representing a worst-case URLLC scenario with significant interference uncertainty. The channels between the eNBs and the UE are modeled as quasi-static, frequency-flat Rayleigh fading multiple-input single-output (MISO) channels. Since URLLC transmissions employ short packets, the packet duration is typically much shorter than the channel coherence time, making the quasi-static assumption valid and enabling accurate channel quality indicator (CQI) estimation for beamforming and resource allocation [14]. The channel gain vectors from eNB-1 and eNB-2 to the UE are denoted by $\mathbf{h} \in \mathcal{C}^{1\times N_t}$ and $\mathbf{g} \in \mathcal{C}^{1\times N_t}$, respectively, whose elements are modeled as independent complex Gaussian random variables (RVs) with zero mean and unit variance.

During the measurement slot ($t = 0$), eNB-1 transmits a pilot symbol and the UE measures the SINR and feeds back the CQI. The received signal is

$$y_0 = \mathbf{hp}s_0 + \mathbf{gu}_0 x_0 + n_0, \tag{1}$$

where n_0 denotes the AWGN with zero mean and variance σ_n^2, s_0 is the pilot symbol with $\mathbb{E}[|s_0|^2] = \rho_s$, and x_0 is the interference signal with $\mathbb{E}[|x_0|^2] = \rho_{\mathcal{I}}$. The vector $\mathbf{p} \in \mathbb{C}^{N_t\times 1}$ denotes the maximum ratio transmission (MRT) beamforming vector of eNB-1, while $\mathbf{u}_0 \in \mathbb{C}^{N_t\times 1}$ represents the beamforming vector of eNB-2 corresponding to its scheduled user. From the perspective of the URLLC UE, $\mathbf{u}_0$ is a complex vector drawn uniformly from the N_t-dimensional complex space. At time $t = 1$, eNB-1 transmits the payload. As eNB-2 may serve different UEs over time, its beamforming vector varies, introducing additional interference randomness. The received signal is given by

$$y_1 = \mathbf{hp}s_1 + \mathbf{gu}_1 x_1 + n_1, \tag{2}$$

where s_1 is the information symbol with $\mathbb{E}[|s_1|^2] = \rho_s$, x_1 is the interference signal with $\mathbb{E}[|x_1|^2] = \rho_{\mathcal{I}}$, n_1 is AWGN with variance σ_n^2, and $\mathbf{u}_1 \in \mathcal{C}^{N_t\times 1}$ is the beamforming vector of eNB-2. From (1), the measured SINR is

$$\gamma_0 = \frac{\rho_s|\mathbf{h}|^2}{\rho_{\mathcal{I}}|\mathbf{g}^{\mathrm{T}}\mathbf{u}_0|^2 + \lambda_0}, \tag{3}$$

where λ_0 denotes the instantaneous noise power, which follows exponential distribution with mean σ_n^2. Similarly, the SINR during payload transmission is

$$\gamma_1 = \frac{\rho_s|\mathbf{h}|^2}{\rho_{\mathcal{I}}|\mathbf{g}^{\mathrm{T}}\mathbf{u}_1|^2 + \lambda_1}, \tag{4}$$

where λ_1 denotes the instantaneous noise power, having exponential distribution with mean σ_n^2. These SINR expressions are used to characterize SINR variations across consecutive time slots for backoff-based link adaptation.

III. Proposed Link Adaptation Scheme

A. Backoff Analysis

Direct rate selection based on the measured SINR may result in packet loss due to time-varying interference and noise. To address this uncertainty, a backoff margin is introduced by reducing the effective SINR used for rate adaptation. For measured SINR γ_0 and target packet failure probability P_{fail}, the backoff is given by

$$\Pr\left(\gamma_1 \le \frac{\gamma_0}{\mathcal{B}}\right) \le P_{fail}, \tag{5}$$

where $\mathcal{B} \ge 1$. The backoff depends only on the statistics of the interference and additive noise levels. Further, (5) can be rewritten as

$$F_R\left(\frac{1}{\mathcal{B}}\right) \le P_{fail}, \tag{6}$$

where $F_R\left(\frac{1}{\mathcal{B}}\right) = P_r\left(R \le \frac{1}{\mathcal{B}}\right)$ and $F_R(\cdot)$ denotes the cumulative distribution function (CDF) of RV $R = \frac{\gamma_1}{\gamma_0}$. Further, using (6), the desired backoff can be obtained as

$$\mathcal{B} = \frac{1}{F_R^{-1}\left(P_{fail}\right)}, \tag{7}$$

where $F_R^{-1}(\cdot)$ denotes the inverse CDF. This backoff $\mathcal{B}$ can be obtained by inverting the CDF of the SINR changes R in two consecutive time slots.

In addition, based on the selected backoff, the transmission rate can be adapted to achieve the target link reliability. The achievable transmission rate is given by [14]:

$$r_t \approx (1 - P_{fail})\log_2\left(1 + \frac{\gamma_0}{\mathcal{B}}\right) + \mathcal{O}\left(\frac{\log_2(m)}{m}\right), \tag{8}$$

where asymptotic notation $\mathcal{O}(\cdot)$ can be approximated as $\frac{\log_2(m)}{2m}$. Using (7), eNB-1 schedules the payload transmission with a rate r_t bits per second per hertz (bps/Hz).

B. Statistical Distribution of ratio of SINRs

To capture SINR variations, we study the statistical distribution of the SINR ratio across consecutive time slots. Under quasi-static channels with time-varying interference and noise, these fluctuations are determined by interference and noise statistics. The CDF of the SINR ratio characterizes the probability of deviation from the previously measured SINR. The SINR ratio is given by

$$R = \frac{\gamma_1}{\gamma_0} = \frac{Y}{X} = \frac{\mathcal{I}_0 + \lambda_0}{\mathcal{I}_1 + \lambda_1}, \tag{9}$$

where $\mathcal{I}_0 = \rho_{\mathcal{I}}\left|\mathbf{g}^{\mathrm{T}}\mathbf{u}_0\right|^2$ and $\mathcal{I}_1 = \rho_{\mathcal{I}}\left|\mathbf{g}^{\mathrm{T}}\mathbf{u}_1\right|^2$. The ℓ_2-norm square of the interfering channel is $P_g = \|\mathbf{g}\|_2^2$. The interference power levels can be written as $\mathcal{I}_0 = \rho_{\mathcal{I}}P_g\left|\tilde{\mathbf{g}}^{\mathrm{T}}\mathbf{u}_0\right|^2$ and $\mathcal{I}_1 = \rho_{\mathcal{I}}P_g\left|\tilde{\mathbf{g}}^{\mathrm{T}}\mathbf{u}_1\right|^2$, where $\tilde{\mathbf{g}} = \frac{\mathbf{g}}{\sqrt{P_g}}$. Based on [11], [13],

the probability distribution function (PDF) of the interference power $\mathcal{I}_0$ is given by

$$f_{\mathcal{I}_0}(\mathcal{I}) = \left(\frac{N_t-1}{\alpha}\right)\left(1-\frac{\mathcal{I}}{\alpha}\right)^{N_t-2}, \quad 0 \le \mathcal{I} \le \alpha \tag{10}$$

where $\alpha = \rho_{\mathcal{I}} P_g$. The RV $\mathcal{I}_1$ is distributed similar to $\mathcal{I}_0$. The PDF of RV Y can be obtained as

$$f_Y(y) = \int_0^{\infty} f_{\mathcal{I}_0}(\gamma-\lambda) f_{\lambda_0}(\lambda)\, d\lambda, \tag{11}$$

where $f_{\lambda_0}(\lambda) = \frac{1}{\sigma_n^2} e^{-\frac{\lambda}{\sigma_n^2}}, \lambda \ge 0$. By substituting the PDFs of $f_{\lambda_0}(\lambda)$ and $f_{\mathcal{I}_0}(\mathcal{I})$ into (11), and solving the integral, we get the PDF of Y given in Lemma 1.

Lemma 1. *The PDF of the interference-plus-noise power Y is given as*

$$f_Y(y) = \begin{cases} \nu\, y^n\, \Upsilon\left(k+1, \frac{y}{\sigma_n^2}\right), & 0 \le y \le \alpha \\ \nu\, y^n\, \Gamma\left(k+1, \frac{y-\alpha}{\sigma_n^2}\right), & y > \alpha, \end{cases} \tag{12}$$

where $\Upsilon(\cdot,\cdot)$ denotes the lower incomplete gamma function, $\Gamma(\cdot,\cdot)$ denotes the upper incomplete gamma function and

$$\nu = (N_t-1)\sum_{k=0}^{(N_t-2)}\sum_{n=0}^{(N_t-k-2)}\binom{N_t-2}{k}\binom{N_t-k-2}{n} \cdot \left(\frac{1}{\alpha}\right)^{k+n+1}(-1)^n\,\sigma_n^{2k}.$$

Proof. See Appendix A ∎

The CDF of interference-plus-noise power RV Y can be obtained as

$$F_Y(y) = P_r(Y \le y) = \int_0^y f_Y(y)\, dy. \tag{13}$$

By substituting (12) into (13) and evaluating the integral, the CDF of the RV Y is obtained as stated in Lemma 2.

Lemma 2. *The CDF of the interference-plus-noise power Y is given as follows:*

$$F_Y(y) = \begin{cases} \nu\left(\frac{y^{n+1}}{n+1}\Upsilon\left(k+1, \frac{y}{\sigma_n^2}\right) - \frac{\sigma_n^{2n+2}}{n+1}\Upsilon\left(n+k+2, \frac{y}{\sigma_n^2}\right)\right), & y \le \alpha \\ \mu\left(\Upsilon\left(n+q+1, \frac{y}{\sigma_n^2}\right) - \Upsilon\left(n+q+1, \frac{\alpha}{\sigma_n^2}\right)\right), & y > \alpha \end{cases} \tag{14}$$

where $\mu = \nu k!\, e^{\frac{\alpha}{\sigma_n^2}} \sum_{l=0}^{k}\sum_{q=0}^{l} \frac{1}{l!}\sigma_n^{2(n+q-l+1)}\binom{l}{q}(-\alpha)^{l-q}$.

Proof. See Appendix B ∎

Remark 1. *The RV X follows the same distribution as the RV Y.*

Since the RV R is defined as the ratio of independent and identically distributed (i.i.d.) RVs, its CDF satisfies the symmetry property $F_R(r) = 1 - F_R(1/r)$, as discussed in [13]. In particular, this implies $F_R(1) = 0.5$. Thus, it is sufficient to determine $F_R(r)$ either for $r < 1$ or for $r > 1$. The CDF of RV R can be obtained as

$$F_R(r) = \Pr(y < r\,x) = \int_0^{\infty} F_Y(rx) f_X(x) dx, \; r \le 1. \tag{15}$$

By substituting the PDF and CDF of the interference-plus-noise RV into (15) and evaluating the resulting integral, we obtain the CDF of R. The piecewise evaluation of the integral in (15) results from the piecewise distribution of the interference-plus-noise RV. Specifically, the interference power is bounded within $[0, \alpha]$, while the noise power is unbounded. Consequently, the joint integration region is divided into cases depending on whether the interference-plus-noise realization is below or above the threshold α.

For Case I ($0 \le x \le \alpha$ and $0 \le y \le rx$), substituting $F_Y(y)$ and $f_X(x)$ in (15) yields the following expression for the CDF of R:

$$F_R^{(I)}(r) = \frac{\nu v r^{n+1}}{n+1}\int_0^{\alpha} x^{m+n+1}\Upsilon\left(k+1, \frac{rx}{\sigma_n^2}\right)\Upsilon\left(t+1, \frac{x}{\sigma_n^2}\right)dx - \frac{\nu v \sigma_n^{2n+2}}{n+1}\int_0^{\alpha} x^m \Upsilon\left(n+k+2, \frac{rx}{\sigma_n^2}\right)\Upsilon\left(t+1, \frac{x}{\sigma_n^2}\right)dx, \tag{16}$$

where,

$$v = (N_t-1)\sum_{t=0}^{(N_t-2)}\sum_{m=0}^{(N_t-t-2)}\binom{N_t-2}{t}\binom{N_t-t-2}{m} \cdot \left(\frac{1}{\alpha}\right)^{t+m+1}(-1)^m\,\sigma_n^{2t}$$

For Case II ($\alpha \le x \le \frac{\alpha}{r}$ and $0 \le y \le rx$), the CDF of R is given as

$$F_R^{(II)}(r) = \frac{\nu v r^{n+1}}{n+1}\int_{\alpha}^{\frac{\alpha}{r}} x^{m+n+1}\Upsilon\left(k+1, \frac{rx}{\sigma_n^2}\right)\Gamma\left(t+1, \frac{x-\alpha}{\sigma_n^2}\right)dx - \frac{\nu v \sigma_n^{2n+2}}{n+1}\int_{\alpha}^{\frac{\alpha}{r}} x^m \Upsilon\left(n+k+2, \frac{rx}{\sigma_n^2}\right)\Gamma\left(t+1, \frac{x-\alpha}{\sigma_n^2}\right)dx. \tag{17}$$

For Case III ($\frac{\alpha}{r} \le x \le \infty$ and $0 \le y \le \alpha \;\cup\; \alpha < y \le rx$), (15) can be rewritten as

$$F_R^{(III)}(r) = \int_{\frac{\alpha}{r}}^{\infty} F_Y(\alpha) f_X(x) dx + \int_{\frac{\alpha}{r}}^{\infty}\int_{\alpha}^{rx} f_Y(y) f_X(x) dy\, dx. \tag{18}$$

By substituting the CDF and PDF of RVs Y and X in (18), and solving it, we have

$$F_R^{(III)}(r) = \frac{\nu v}{n+1}\left(\alpha^{n+1}\Upsilon\left(k+1, \frac{\alpha}{\sigma_n^2}\right) - \sigma_n^{2n+2}\Upsilon\left(n+k+2, \frac{\alpha}{\sigma_n^2}\right)\right) \cdot \int_{\frac{\alpha}{r}}^{\infty} x^m \Gamma\left(t+1, \frac{x-\alpha}{\sigma_n^2}\right)dx + \mu v \int_{\frac{\alpha}{r}}^{\infty} x^m \Gamma\left(t+1, \frac{x-\alpha}{\sigma_n^2}\right) \cdot \left(\Upsilon\left(n+q+1, \frac{rx}{\sigma_n^2}\right) - \Upsilon\left(n+q+1, \frac{\alpha}{\sigma_n^2}\right)\right)dx. \tag{19}$$

Since the integrals in (16), (17), and (19) do not admit closed-form solutions, their numerical values are evaluated using the software *Mathematica*. The CDF of R can be expressed as $F_R(r) = F_R^{(I)} + F_R^{(II)} + F_R^{(III)}$. For $r \ll 1$, it is observed that $F_R^{(I)} > F_R^{(II)} > F_R^{(III)}$. From a URLLC perspective, the primary interest lies in the left-tail behaviour of the RV R, which corresponds to significant SINR drops. Therefore, under the dominance of Case I, the CDF can be approximated

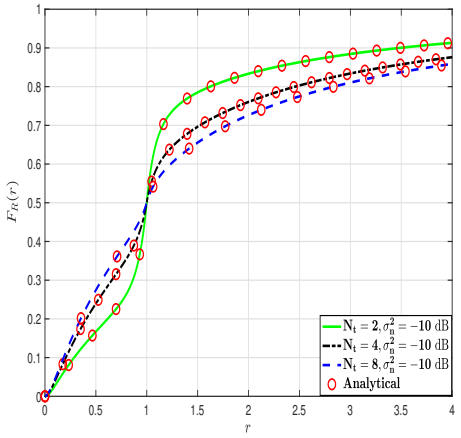

Fig. 1: CDF plot for ratio of SINRs

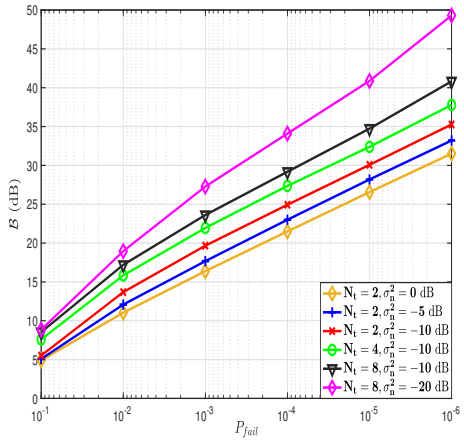

Fig. 2: Backoff vs P_{fail} plot for various values of N_t and σ_n^2.

as $F_R(r) \approx F_R^{(I)}$, particularly in interference-limited scenarios where SINR fluctuations are primarily governed by interference variability.

IV. Numerical Analysis

This section presents numerical results illustrating the impact of interference and noise on URLLC reliability. The simulation parameters are set to $\rho_s = \rho_{\mathcal{I}} = 0$ dB and blocklength size $m = 200$. Results are validated through Monte Carlo simulations with 10^7 channel realizations.

Fig. 1 shows the distribution of SINR variability across two consecutive time slots under interference and noise. The CDF shows that r is concentrated around one due to the noise statistic has zero mean. As N_t increases, interference variability increases, smoothing the CDF and increasing the tail probability, which reflects greater uncertainty in the interference power experienced by the URLLC UE.

Fig. 2 illustrates the required backoff for a target packet error probability for different N_t and σ_n^2. For $N_t = 2$, the backoff increases as the additive noise variance decreases. At lower noise levels, SINR fluctuations are dominated by time-varying interference, which increases the probability that the payload SINR falls below its estimated value. For $\sigma_n^2 = -10$ dB, the required backoff further increases with N_t due to increasing interference uncertainty with N_t.

Fig. 3 shows the transmission rate versus P_{fail} for different N_t and σ_n^2. For $\sigma_n^2 = -10$ dB, increasing N_t improves the transmission rate, while higher noise power reduces it. Time-varying interference from uncoordinated beamforming at eNB 2 and additive noise also reduce the effective beamforming gain of eNB 1, causing rate fluctuations and emphasizing the need for effective link adaptation.

V. Conclusion

We investigate the impact of interference and noise on URLLC link reliability. The statistical distribution of the interference-plus-noise power and its ratio across consecutive time slots is analytically derived to characterize SINR

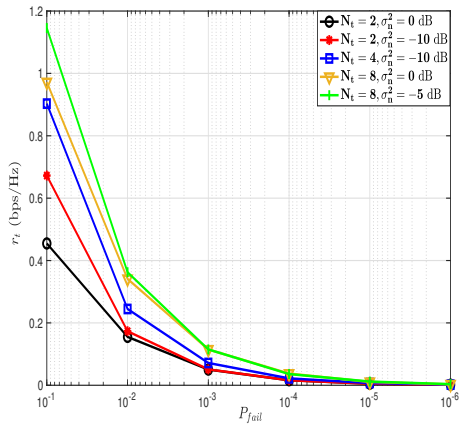

Fig. 3: Transmission rate vs P_{fail} for different N_t and σ_n^2.

variability under quasi-static fading. The results show that increasing the number of transmit antennas at the interferer increases interference uncertainty, thereby requiring a larger backoff margin. In addition, reducing the additive noise variance further increases the required backoff. This increased backoff reduces the effective beamforming gain in the low P_{fail} regime, resulting in lower transmission rates to maintain the target reliability in non-stationary environments. Overall, the proposed analytical framework provides insights into SINR fluctuations under dynamic interference and noise, enabling reliability-aware link adaptation for URLLC.

Future work may extend this study to multi-interferer scenarios, incorporate mobility-induced channel aging, and develop optimal rate adaptation policies under stricter latency and reliability constraints.

Appendix A
Proofs of Lemma 1

For Case I ($0 \leq y \leq \alpha$), from (11), the PDF of the RV Y can be expressed as

$$f_Y(y) = \left(\frac{N_t - 1}{\alpha\, \sigma_n^2}\right) \int_0^y \left(1 - \frac{y - \lambda}{\alpha}\right)^{N_t - 2} e^{-\frac{\lambda}{\sigma_n^2}}\, d\lambda \quad (20)$$

Applying the binomial expansion in (20), we obtain:

$$f_Y(y) = c\left(1-\frac{y}{\alpha}\right)^{N_t-k-2}\int_0^y \lambda^k\, e^{-\frac{\lambda}{\sigma_n^2}}\, d\lambda, \quad (21)$$

where $c = \left(\frac{N_t-1}{\sigma_n^2}\right)\sum_{k=0}^{N_t-2}\binom{N_t-2}{k}\left(\frac{1}{\alpha}\right)^{k+1}$. After evaluating the integral in (21) using [15, Eq. 3.381.1], the result can be expressed as:

$$f_Y(y) = c\left(1-\frac{y}{\alpha}\right)^{N_t-k-2}\sigma_n^{2k+2}\Upsilon\left(k+1, \frac{y}{\sigma_n^2}\right), \quad (22)$$

where $\Upsilon(\cdot,\cdot)$ is the lower incomplete gamma function. After applying the binomial expansion in (22) and plugging the value of c, the PDF of Y is obtained as given in (12) for Case I.

For Case II ($y \geq \alpha$), from (11), the PDF of the RV Y after applying binomial expansion can be expressed as

$$f_Y(y) = c\left(1-\frac{y}{\alpha}\right)^{N_t-k-2}\int_{y-\alpha}^{\infty} \lambda^k\, e^{-\frac{\lambda}{\sigma_n^2}}\, d\lambda. \quad (23)$$

After evaluating the integral in (21) using [15, Eq. 3.381.3], the result can be expressed as:

$$f_Y(y) = c\left(1-\frac{y}{\alpha}\right)^{N_t-k-2}\sigma_n^{2k+2}\Gamma\left(k+1, \frac{y-\alpha}{\sigma_n^2}\right), \quad (24)$$

where $\Gamma(\cdot,\cdot)$ denotes the upper incomplete gamma function. After applying the binomial expansion in (24) and putting in the value of c, the PDF of Y is given in (12).

Appendix B
Proofs of Lemma 2

For Case I ($0 \leq y \leq \alpha$), from (13) with change of variable $y \to u$, the CDF Y can be expressed as follows:

$$F_Y(y) = \nu\int_0^y u^n\, \Upsilon\left(k+1, \frac{u}{\sigma_n^2}\right) du. \quad (25)$$

By using the definition of the lower incomplete gamma function, (25) can be expressed as

$$F_Y(y) = \nu\int_0^y\int_0^u u^n t^k e^{-t} dt\, du, \quad (26)$$

where the region on the integral is $0 \leq t \leq u \leq y$. By interchanging the order of integration $t \leq u \leq y, 0 \leq t \leq y$, the integral in (26) can be rewritten as:

$$F_Y(y) = \nu\int_0^y t^k e^{-t}\left(\int_t^y u^n\, du\right) dt. \quad (27)$$

After solving the inner integral in (27), we have

$$F_Y(y) = \frac{\nu}{n+1}\left(y^{n+1}\int_0^y t^k e^{-t} dt - \int_0^y t^{k+n+1} e^{-t} dt\right). \quad (28)$$

After evaluating the integral in (28) using [15, Eq. 3.381.1], the CDF of Y for Case I is given in Lemma 2.

For Case II ($y > \alpha$), $F_Y(y)$ is given as

$$F_Y(y) = \nu\int_\alpha^u u^n \Gamma\left(k+1, \frac{u-\alpha}{\sigma_n^2}\right) du. \quad (29)$$

By applying the relation $\Gamma(k,x) = \Gamma(k) - \Upsilon(k,x)$ in (29), and evaluating the first integral, we obtain

$$F_Y(y) = \frac{\nu\Gamma(k+1)}{n+1}\left(y^{n+1}-\alpha^{n+1}\right) - \nu\underbrace{\int_\alpha^y u^n \Upsilon\left(k+1, \frac{u-\alpha}{\sigma_n^2}\right) du}_{I(y)}. \quad (30)$$

Using $\Upsilon(k,x) = (k-1)!\left(1-e^{-x}\sum_{l=0}^{k-1}\frac{x^l}{l!}\right)$ in (30) and after solving the first integral, $I(y)$ can be written as

$$I(y) = \frac{k!}{n+1}\left(y^{n+1}-\alpha^{n+1}\right) - \kappa\underbrace{\int_\alpha^y u^{n+r} e^{-\frac{u}{\sigma_n^2}} du}_{I_1(y)}, \quad (31)$$

where $\kappa = k! e^{\frac{\alpha}{\sigma_n^2}}\sum_{l=0}^{k}\sum_{q=0}^{l}\frac{1}{l!\sigma_n^{2l}}\binom{l}{q}(-\alpha)^{l-q}$. By splitting integral in (31) and using [15, Eq. 3.381.1], we get

$$I_1(y) = \sigma_n^{2(n+q+1)}\left(\Upsilon\left(n+q+1, \frac{y}{\sigma_n^2}\right) - \Upsilon\left(n+q+1, \frac{\alpha}{\sigma_n^2}\right)\right). \quad (32)$$

By substituting (32) into (31), and subsequently (31) into (30), the CDF of Y for Case II is obtained as stated in Lemma 2.

Acknowledgment

This work was supported by the FRS Grant (MISC-0263), IIT (ISM) Dhanbad, Jharkhand, India.

References

[1] Z. Li et al., "5G URLLC: Design challenges and system concepts," *15th Int. Symp. on Wirel. Communi. Systems (ISWCS)*, Lisbon, Portugal, 2018, pp. 1-6.

[2] C. -H. Yu, A. Hellsten, and O. Tirkkonen, "Rate adaptation of AMC/HARQ systems with CQI errors," *IEEE 71st Vehicular Technology Conference*, Taipei, Taiwan, 2010, pp. 1-5.

[3] H. Shariatmadari et al., "Link adaptation design for ultra-reliable communications," *IEEE Int. Conf. on Communi. (ICC)*, Kuala Lumpur, Malaysia, 2016, pp. 1-5.

[4] H. Shariatmadari et al., "Optimized transmission and resource allocation strategies for ultra-reliable communications," *IEEE Int. Symp. on Pers., Indoor, and Mobile Radio Communi. (PIMRC)*, Valencia, Spain, 2016, pp. 1-6.

[5] H. Shariatmadari, R. Duan, S. Iraji, R. Jäntti, Z. Li and M. A. Uusitalo, "Asymmetric ACK/NACK detection for ultra - reliable low-latency communications," *European Conference on Networks and Communications (EuCNC)*, Ljubljana, Slovenia, 2018, pp. 1-5.

[6] A. Kosta, N. Pappas, and V. Angelakis, "Age of information: A new concept, metric, and tool," *ser. Foundations and Trends in Networking Series.* Now Publishers, 2017.

[7] B. Singh et al., "Ultra-reliable communication in a factory environment for 5G wireless networks: link level and deployment study,"in Proc. *IEEE Int. Symp. on Personal, Indoor and Mobile Radio Commun. (PIMRC)*, Valencia (Spain), Sep. 2016, pp 1-5.

[8] A. Brighente, J. Mohammadi and P. Baracca, "Interference distribution prediction for link adaptation in ultra-reliable low-latency communications," *IEEE 91st Vehicular Technology Conference (VTC2020-Spring)*, Antwerp, Belgium, 2020, pp. 1-7.

[9] F. Salehi et al., "Ultra-high reliability by predictive interference management using extreme value theory," *IEEE International Conference on Communications (ICC)*, Montreal, Canada, 2025, pp. 2538-2543.

[10] U. Oruthota, F. Ahmed, and O. Tirkkonen, "Ultra-reliable link adaptation for downlink MISO transmission in 5G cellular networks," Information, vol. 7, no. 1, p. 14, Mar 2016.

[11] K. K. Mukkavilli et al., "On beamforming with finite rate feedback in multiple-antenna systems," *IEEE Trans. Inf. Theory*, vol. 49, no. 10, pp. 2562–2579, Oct. 2003.

[12] U. Singh and O. Tirkkonen, "Link-Adaptation for Downlink MIMO URLLC Transmissions," *IEEE Wireless Communications and Networking Conference (WCNC), Dubai, United Arab Emirates, 2024*, pp. 1-6.

[13] U. Singh and O. Tirkkonen, "Robust link adaptation in multiantenna URLLC systems wth flashlight interference," *IEEE Communications Letters*, vol. 28, no. 10, pp. 2432-2436, Oct. 2024.

[14] W. Yang, G. Durisi, T. Koch, and Y. Polyanskiy, "Quasi-static multipleantenna fading channels at finite blocklength," IEEE Trans. Inf. Theory, vol. 60, no. 7, pp. 4232–4265, Jul. 2014.

[15] I. Gradshteyn and I.Ryzhik, "Table of integrals, series, and products," *Academic Press,San Diego,California,7th ed.*, 2007.